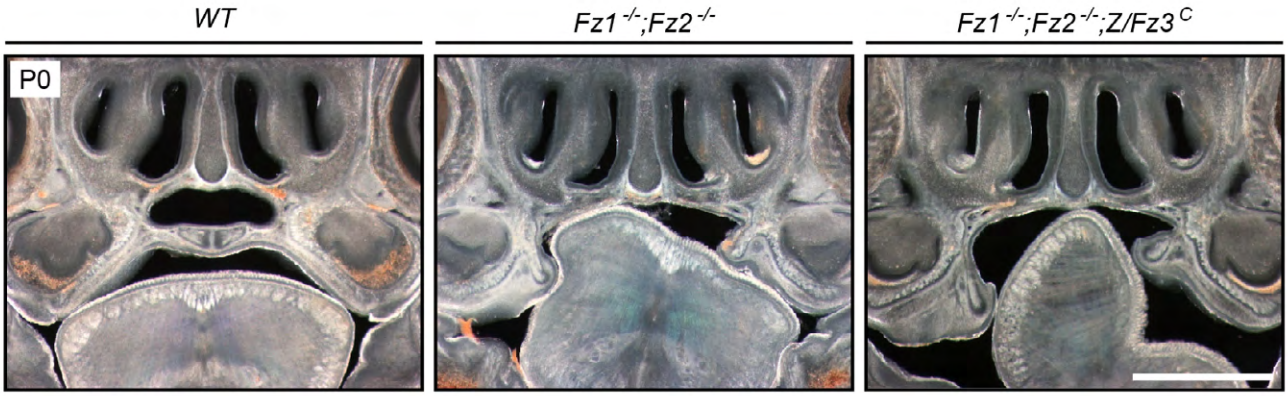

Figure S1. Failure of *Z/Fz3*^{C} to rescue the palate closure defect in *Fz1*$^{-/-}$*;Fz2*$^{-/-}$ embryos.

Coronal sections through the head at P0 show the tongue (bottom), the palate (middle), and the nasal cavities and olfactory turbinates (top). In *Fz1*$^{-/-}$*;Fz2*$^{-/-}$ and *Fz1*$^{-/-}$*;Fz2*$^{-/-}$*;Z/Fz3*^{C} embryos, the failure of palate closure allows the tongue to protrude upward into the nasal cavity. Scale bar, 1 mm.

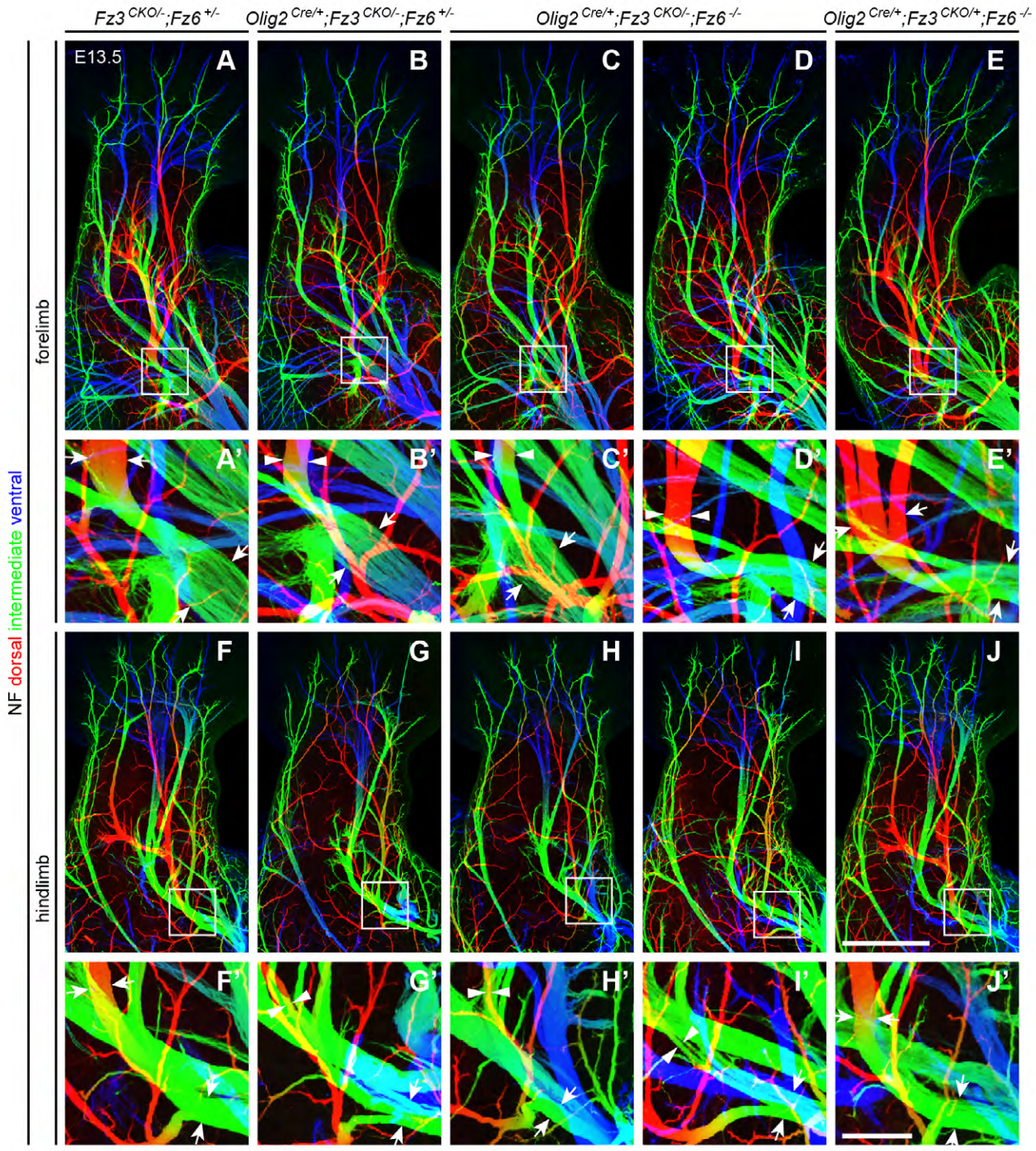

Figure S2. *Fz6* does not play a redundant role with *Fz3* in motor axon innervation of the dorsal limb.

(A-E') NF immunostaining of whole-mount E13.5 forelimbs. Boxed regions in (A-E) are magnified in (A'-E'). In *Olig2$^{Cre/+}$;Fz3$^{CKO/-}$;Fz6$^{+/-}$* and *Olig2$^{Cre/+}$;Fz3$^{CKO/-}$;Fz6$^{-/-}$* forelimbs, the dorsal nerve is thinned to similar extents (compare regions between arrows and arrowheads in B and B' vs. C-D'; limbs from two *Olig2$^{Cre/+}$;Fz3$^{CKO/-}$;Fz6$^{-/-}$* embryos, 0803-6 and 0804-3, are shown). In *Olig2$^{Cre/+}$;Fz3$^{CKO/+}$;Fz6$^{-/-}$* forelimbs (E and E') the dorsal nerve thickness is indistinguishable from the *WT* control (compare regions between arrows in A and A' vs. E and E'). Depth within the Z-stack along the dorsal to ventral axis is color-coded from red to blue. In this figure, arrows show normal nerve widths and arrowheads show reduced widths.

(F-J') NF immunostaining of whole-mount E13.5 hindlimbs. Boxed regions in (F-J) are magnified in (F'-J'). In *Olig2$^{Cre/+}$;Fz3$^{CKO/-}$;Fz6$^{+/-}$* and *Olig2$^{Cre/+}$;Fz3$^{CKO/-}$;Fz6$^{-/-}$* hindlimbs, the dorsal nerve is thinned to similar extents (compare regions between arrows and arrowheads in G and G' vs. H-I'). In *Olig2$^{Cre/+}$;Fz3$^{CKO/+}$;Fz6$^{-/-}$* hindlimbs the dorsal nerve thickness is indistinguishable from the *WT* control (compare regions between arrows in F and F' vs. J and J'). Depth within the Z-stack along the dorsal to ventral axis is color-coded from red to blue. Scale bars: (J), 500 μm; (J'), 100 μm.

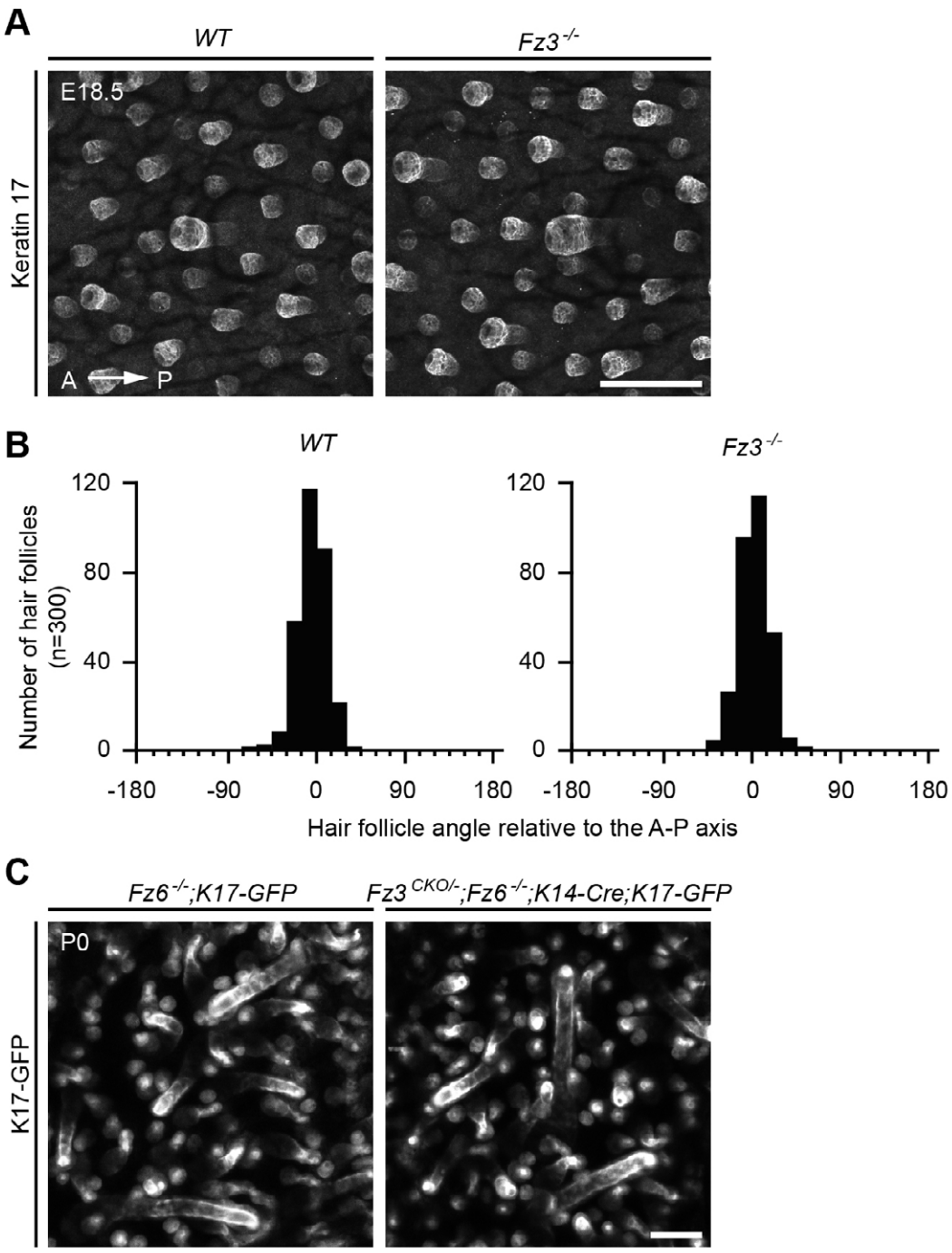

Figure S3. Loss of *Fz3* has no effect on hair follicle orientation at E18.5.

(A) Whole-mount back skin from *WT* and *Fz3*$^{-/-}$ E18.5 embryos immunostained for K17 to visualize hair follicles. A, anterior; P, posterior. Scale bars, 200 µm.

(B) Quantification of hair follicle orientations relative to the A-P axis. Both distributions cluster tightly around zero degrees.

(C) At P0, the hair follicle orientation phenotype produced by combined loss of *Fz6* globally and *Fz3* in the epidermis is indistinguishable from the phenotype produced by global loss of *Fz6*. Whole-mount back skin from *Fz6*$^{-/-}$*;K17-GFP* and *Fz3*$^{CKO/-}$*;Fz6*$^{-/-}$*;K14-Cre;K17-GFP* mice at P1 was imaged for GFP to visualize hair follicles. Scale bar, 100 µm.

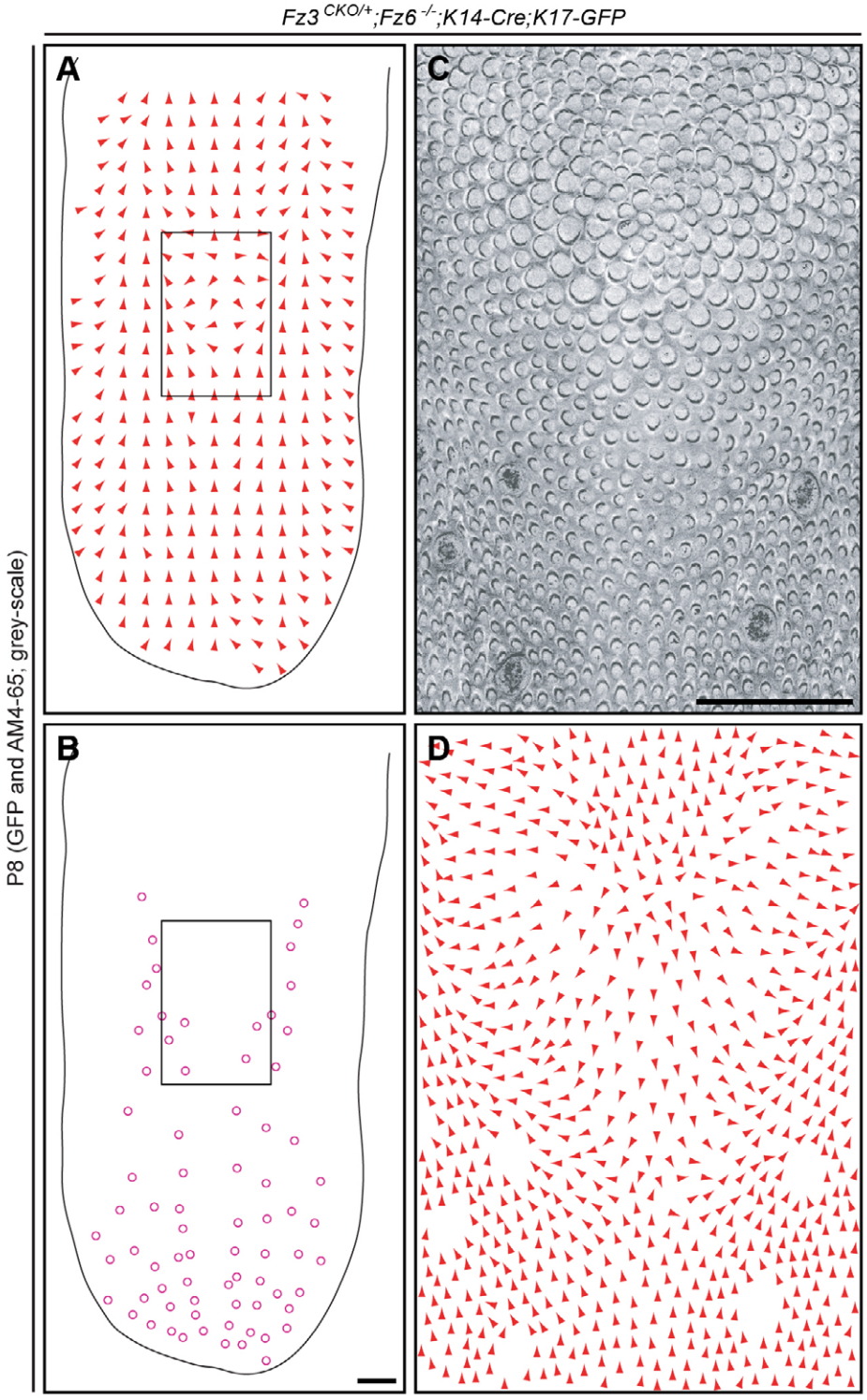

Figure S4. Lingual papillae in and around the patterning center show contiguous variations in orientation.

(A-D) the dorsal surface of a *Fz3*$^{CKO/+}$*;Fz6*$^{-/-}$*;K14-Cre;K17-GFP* tongue at P8 showing the global orientation of lingual papillae (A) and the locations of taste buds (B); both patterns match those of *WT* tongues. The tongue is outlined in black. Anterior is down. The grey scale image of epithelial GFP and AM4-65 dye fluorescence highlights the structure of the papillae. The region enclosed in the black rectangles in (A) and (B) is enlarged in (C) and (D). The orientation of each papilla in (C) is indicated with an arrowhead in (D). The "flower" pattern is present along the midline near the top of the images in (C) and (D), and the point of confluence of posterior and anterior facing papillae is present below the center of each image. Scale bars, 500 μm.

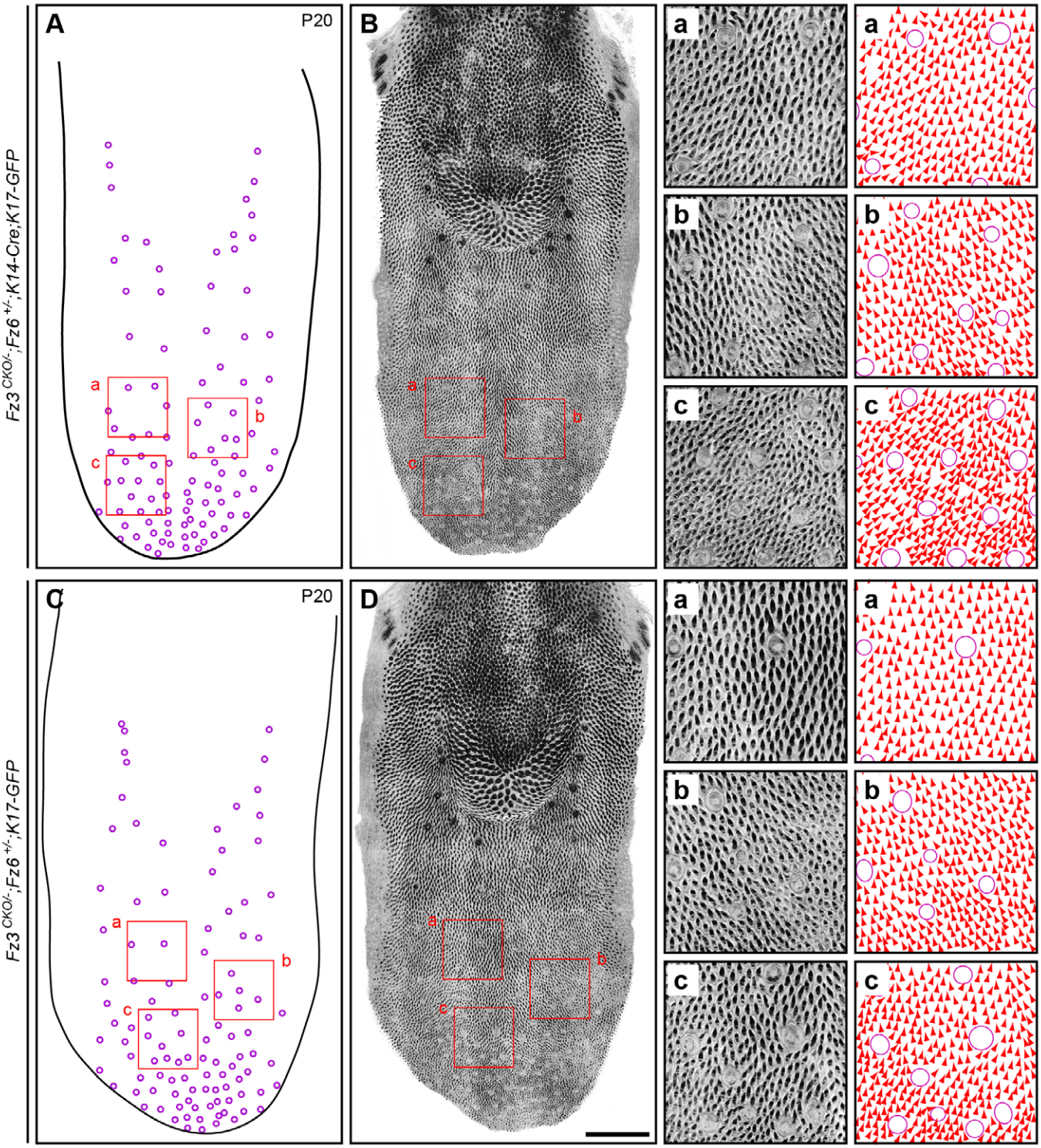

Figure S5. Patterning of lingual papillae is unperturbed in *Fz3$^{CKO/-}$;Fz6$^{+/-}$;K14-Cre* and *Fz3$^{CKO/-}$;Fz6$^{+/-}$* tongues.

(A-D) Dorsal view of a *Fz3$^{CKO/-}$;Fz6$^{+/-}$;K14-Cre;K17-GFP* tongue at P20 (A and B) and a *Fz3$^{CKO/-}$;Fz6$^{+/-}$;K17-GFP* tongue at P20 (C and D) showing the locations of taste buds (A and C) and epithelial morphology with AM4-65 and GFP fluorescence (B and D). In both cases the pattern matches that of *WT* tongues. Anterior is down. The "flower" pattern is present along the midline at ~70% of the distance from the tip to the base of the tongue. The grey scale images to the right (panels a-c) correspond to the locations of the red squares in the low magnification image at left. The orientation of each papilla in (a-c) was scored with an arrowhead. Scale bar, 1 mm.

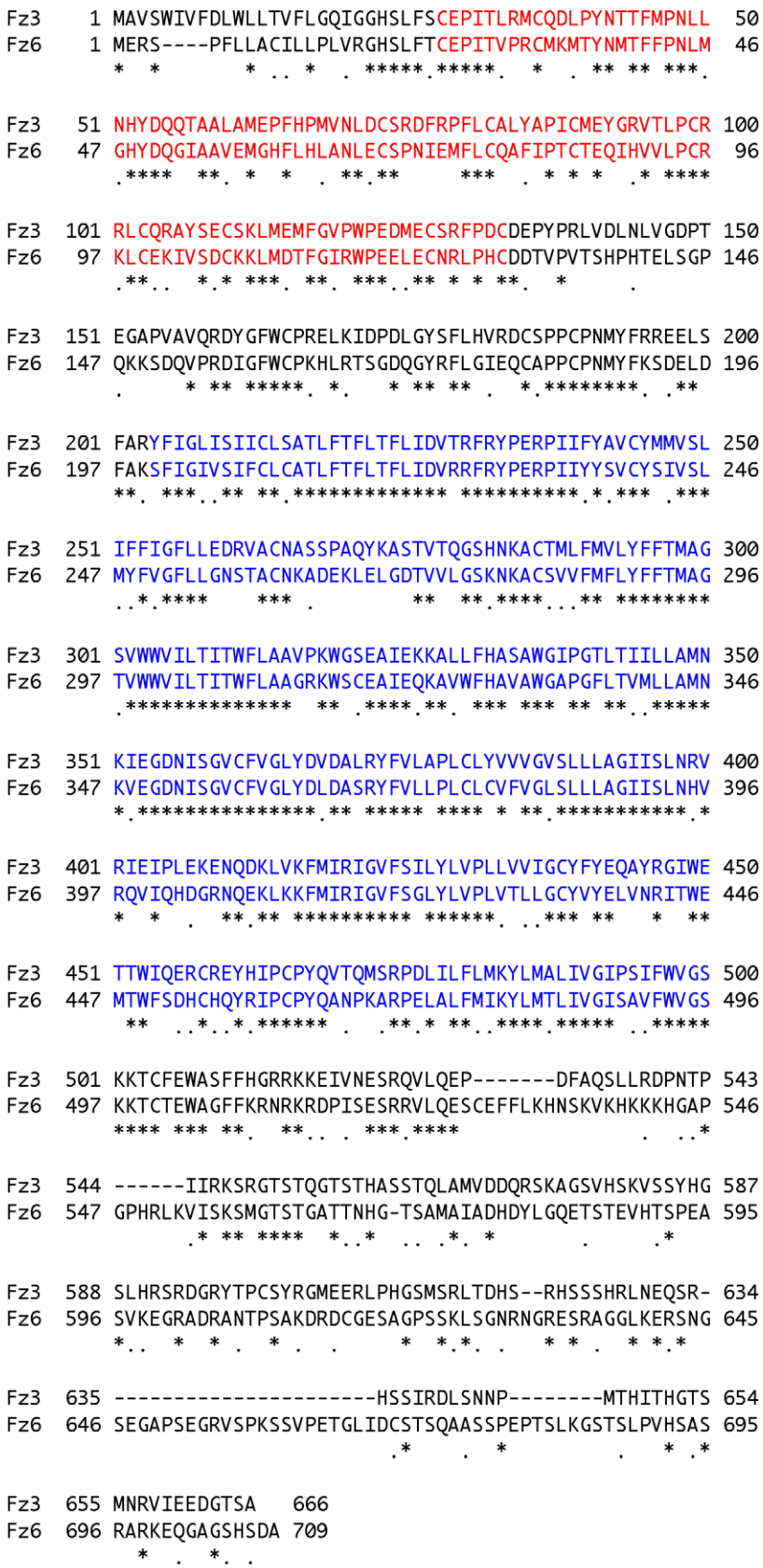

Figure S6. Alignment of mouse Fz3 and Fz6 amino acid sequences.

The ligand-binding cysteine-rich domain is highlighted in red and the predicted transmembrane domain is highlighted in blue. Asterisks indicate amino acid identities and dots indicate similarities.

Supplemental Table 1. Sources for protein sequences used to construct the dendrogram in Figure 7.

Caenorhabditis elegans CFZ-2a: F27E11.3a
Caenorhabditis elegans MOM-5: T23D8.1
Caenorhabditis elegans MIG-1b: Y34D9B.1b

Ciona intestinalis Fz3/6: ENSCINP00000026933

Drosophila melanogaster Fz: FBpp0303135
Drosophila melanogaster Fz2: FBpp0303228
Drosophila melanogaster Fz3: FBpp0111841
Drosophila melanogaster Fz4: FBpp0070977

Gallus gallus (chicken) Fz3: ENSGALP00000026786
Gallus gallus (chicken) Fz6: ENSGALP00000025843

Homo sapiens Fz3: CCDS6069
Homo sapiens Fz6: CCDS6298

Mus musculus Fz3: CCDS27212
Mus musculus Fz6: CCDS27441

Petromyzon marinus (lamprey) Fz6: ENSPMAP00000000914

Takifugu rubripes Fz3: ENSTRUP00000011955
Takifugu rubripes Fz6: ENSTRUP00000017077

Xenopus tropicalis Fz3: ENSXETP00000045728
Xenopus tropicalis Fz6: ENSXETP00000008881

Sources:
CCDS: the Consensus CDS Database
ENS: Ensembl
FB: FlyBase
C. elegans: WormBase